DOI: http://dx.doi.org/10.30684/etj.37.3B.2

Synthesis of ZnO Nanorods on Silicon for Methanol Gas Sensor

Abdulqader D. Faisal
University of Technology, Applied Science Dept., Baghdad, Iraq.
abdulf330@yahoo.com

Mofeed A. Jaleel
University of Technology, Applied Science Dept., Baghdad, Iraq.

Fahad Z. Kamal
University of Technology, Applied Science Dept., Baghdad, Iraq.

Received on: 07/04/2019
Accepted on: 15/05/2019
Published online on: 25/10/2019

Abstract- Zinc Oxide nanorods (ZnO NRs) were successfully synthesized via hydrothermal method. The growth process was conducted with a seed layer concentration of 30 millimolar (mM). The as-synthesized nanostructures were characterized by x-ray diffraction (XRD), scanning electron microscope (SEM), atomic force microscope (AFM), and ultraviolet-visible (UV-VIS) spectrophotometer. The analysis of the present work results revealed pure Wuartzite ZnO hexagonal nanostructures with preferred orientation (002) along c-direction. It was found that the calculated band gap and the crystallite size are 3.2 eV and 53.18 nm respectively. A methanol gas sensor was fabricated based on the annealed ZnO NRs on the silicon substrate. The optimized sensitivity at 250 ppm methanol vapor with fast response and recovery time was achieved. So, ZnO NRs film can serve as a good candidate for a methanol gas sensing device.

Keywords- Hydrothermal, ZnO NRs, Methanol gas sensors, Crystallite size.

How to cite this article: A.D. Faisal, M.A. Jaleel, and F.Z. Kamal, "Synthesis of ZnO Nanorods on Silicon for Methanol Gas Sensor," *Engineering and Technology Journal*, Vol. 37, Part B, No. 3, pp. 74-81, 2019.

1. Introduction

ZnO is one of the important materials in the family of II-VI semiconductors [1], this is due to the direct band gap of 3.37 eV at the ambient conditions [2], also has free exciton binding energy of 60 meV [3]. It is extensively used for transparent films [4]. Due to the extreme superior properties, it was employed for the production of efficient solar cells [5], light emitting diodes [6], chemical sensors [7], piezoelectric devices [8], transparent leads [9], and gas sensor [10]. Recently, many techniques have been used for the synthesis of 1D ZnO nanostructures, such as thermal decomposition [11], microwave activated chemical bath deposition [12], chemical bath deposition [13], vapor-liquid-solid (VLS) growth [14], metal-organic catalyst assisted vapour phase growth [15], direct evaporation [16], chemical vapour deposition (CVD) [17], and template-based methods [18]. However, some of these growth techniques are expensive, substrate restricted. Complex process controlling and high temperature is needed for an industrialized process. Among these techniques, the hydrothermal route is quite favourable [19], which has the advantages of mild synthetic conditions, simple manipulation and large scale-up production. It opens a door for future optoelectronic devices based on ZnO nanostructure arrays [20-25]. Hydrothermal synthesis of ZnO nanostructures has been found in various morphologies, such as nanowires [26], nanoflowers [27], hexagonal nanotubes [28], and nanorods[29] .

The present work was mainly focused on the synthesis of ZnO nanorods via hydrothermal method. It was characterized by x-ray diffraction (XRD), scanning electron microscope (SEM), atomic force microscopy (AFM), and ultraviolet-visible (UV-Vis.) and confirmed the formation of pure Wurtzite ZnO nanorods. The methanol gas sensing performance based on ZnO NRs has grown on a silicon substrate was investigated.

2. Experimental Part

I. Silicon cleaning

Silicon wafer was cut into small pieces with a size of 1 cm x1 cm. These Si substrates were sonicated subsequently with acetone, isopropanol and deionized (DI) water in an ultrasonic bath for 30 minutes for each. Then, the substrates were dried in a nitrogen gas flow.

II. Preparation of ZnO seed layer

ZnO seed layer for hydrothermal growth of the ZnO nanostructures was prepared by drop cast process. The solution for the ZnO seed layer was prepared by adding zinc acetate di-hydrate (purity of 99.99%) with concentration of 30 millimolar (mM) to a 10 mL of ethyl alcohol (purity of 99.99%) in a suitable beaker and continuously stirred using magnetic stirrer at a temperature of 60 oC for 1 hour in order to obtain a full dissolution of the material. The resultant solution

became homogeneous and transparent. This solution was used to deposit the seed layer onto the silicon substrate by drop cast process using a micropipette with a volume of 20 µl/cm^2. Then, the substrate dried with a nitrogen jet and dried with a hot plate at 100 ^{O}C for 5minutes. This process was repeated 4-5 times to ensure a thick layer. Subsequently, the substrates were annealed at 500 °C for 1 h to obtain the ZnO nanocrystals. These ZnO nanocrystals would act as nucleation sites for the growth of ZnO nanostructures .

III. Hydrothermal growth of ZnO nanostructures

The growth solution for the hydrothermal route was prepared by dissolving 25 millimolar (mM) zinc nitrate hexahydrate and 25 mM hexamethylenetetramine (HMTA) in deionized water. Seeded substrates were suspended upside down in a 50 mL growth precursor in a glass vial and left to stand for 2h at 85 °C in the oven. After growth, the resultant samples were removed from the vials, rinsed thoroughly with deionized water to remove any residual reactants and dried in air at normal atmosphere. The grown substrates were subsequently annealed using a programmable muffle furnace (UOT/Applied Science Department/ Research Unit) (model Nabertherm more than heat 30-3000 °C) at 500 °C for 1h in order to remove any organic materials and to decompose the residual zinc nitrate to form ZnO nanocrystals. These ZnO nanocrystals would act as nucleation sites for the growth of ZnO nanostructures.

IV. Characterization

The morphology of the prepared ZnO seed layer was characterized by atomic force microscopy (AFM, Angstrom AA3000-SPM-USA). X-ray diffraction (XRD) analysis of the synthesized ZnO NRs was carried out on Shimadzu XRD-6000. X-ray diffractometer equipped with Cu Kα radiation (λ = 0.15406 nm), employing a scanning speed of 12° min-1 and 2θ ranges from 30° to 60°. The structures of the ZnO nanorods were characterized with a scanning electron microscopy (SEM-VEGA II Tescan – Czech at Nanotechnology Research Center / UOT). The optical properties of the synthesized ZnO nanorods were characterized using the UV-VIS Spectrophotometer (T80 UV-VIS Spectrometer, PG Instruments Ltd. at Applied Science Department).

3. Results and Discussion

I. AFM analysis

The seed layer of ZnO nanocrystals at the concentration of 30 mM was analyzed via AFM technique. The 2D, 3D images and the granularity distribution of the ZnO film are shown in Figure 1. The average grain size, Sa (Average Roughness) and the Sq (Root Mean Square) are 95.85 nm, 1.7 nm, 1.69 nm, respectively.

II. Crystal structure analysis

Figure 2 presents an XRD pattern for ZnO NRs grown on silicon (111) at 30 mM using the hydrothermal method at 85 °C for 2h. The main strong peak can be recognized at 2θ^{0}: 31.9430°, 34.6003°, and 36.4132° and indexed for (100), (002) and (101) reflection planes respectively. Other small peaks at (102) and (110) are also indexed at higher theta. These data are confirmed by standard data issued by JCPDS#36-1451. The dominant orientations are along with the directions represented by the planes (100), (002) and (101). There are no other peaks observed for another material. The Si peak is related to the substrate. This indicates that the synthesized ZnO NRs are highly pure. The resulted data of the XRD of the ZnO nanorods are found to be consistent with the reported data for single crystalline hexagonal ZnO nanorods [30].

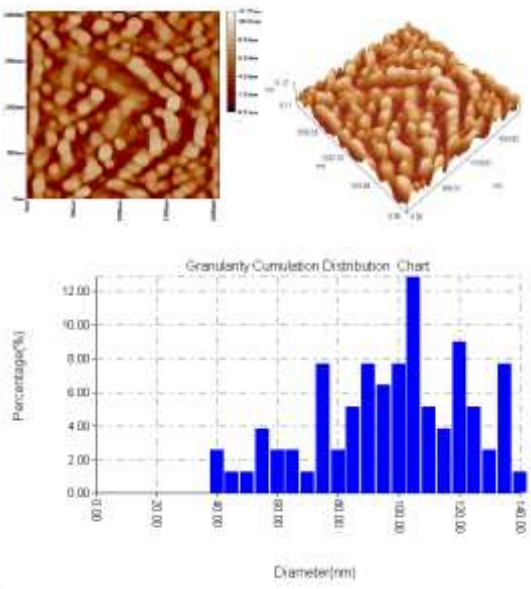

Figure 1: Typical AFM images of ZnO seed layer nanocrystals on Si using 30 mM of zinc acetate dihydrate, a) 2D image; b) 3D image and c) grain size distribution

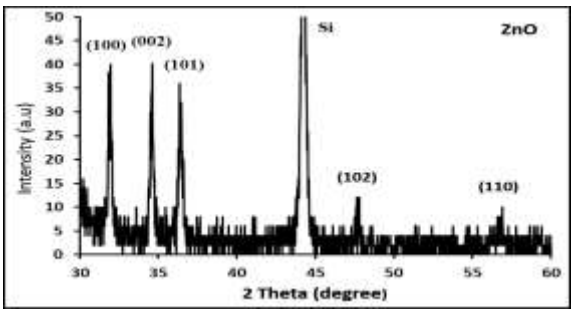

Figure 2: XRD pattern of ZnO NRs grown hydrothermally on Si (111) with a seed layer concentration of 30 mM for 2h and at 85 °C

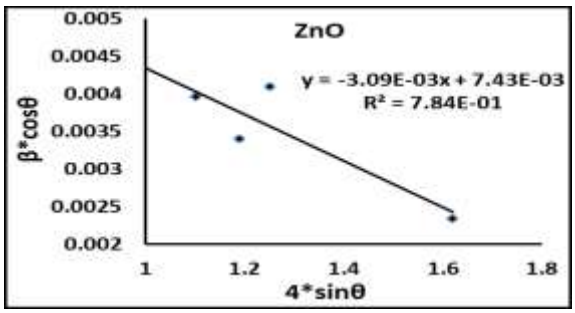

Figure 3: The William-Hall analysis of ZnO NRs grown on silicon

The average crystallite size $D_{(hkl)}$ was calculated using Debye Scherrer's equation: [31]

$$D_{(hkl)}=k.\lambda/\beta 2\Theta\cos\Theta \quad (1)$$

Where k is the shape factor (0.9), λ is the wavelength of Cu Kα radiation, β2Θ is the full width half maximum (FWHM) and Θ is the angle of diffraction. The average crystallite $D_{(D-S)}$ value calculated for ZnO NRs is 44.11 nm. The lattice constants a and c of the hexagonal ZnO Wurtzite structure can be calculated using Bragg's law [32]:

$$a_{(100)}=(\sqrt{1/3})*\lambda/\sin\theta \quad (2)$$

$$c_{(002)}=\lambda/\sin\theta \quad (3)$$

The calculated lattice constants a and c are 3.23255 Å and 5.18062 Å, respectively (c/a=1.6026). These calculated values were compared with the JCPDS card # (36–1451) values: a=3.2498 Å and c=5.2066 Å (c/a=1.6021) for the bulk ZnO.

III. William-Hall plot

The lattice strain and crystallite size were calculated using the following equation [33]:

$$\beta\cos\Theta = 4\varepsilon\sin+\Theta\ (k\lambda/D) \quad (4)$$

Where β, θ, ε are the full width half maximum (FWHM), Bragg's angle and the lattice strain respectively. Figure 3 shows a plot of βcosθ versus 4sinθ for the peaks of ZnO. The data are fitted so that, the strain and particle size are calculated from the slope and y-intercept respectively. The calculated values of the particle size [D (W-H)] and the strain (Ɛ) are 42.23 nm and -3.09x10-3 respectively. From these calculations, it was observed that this strain value is negative which it might be due to the lattice elongation. The comparable calculated values of the crystallite size due to Debye-Sherrer and William- Hall relations are 44.11 nm and 42.23 nm respectively.

IV. SEM analysis

The morphology of ZnO NRs grown hydrothermally on Si at 85 °C for 2h is shown in Figure 4. This figure shows a different magnification of low, medium and high magnified SEM images. It can clearly observe a high density, randomly oriented and well-distributed ZnO nanorods at large area. The estimated lengths of the rods are from 1-2μm, and the measured rod diameters are in the range of 80-100 nm. The cross-section of the straight rods is clearly hexagonal and grown nearly vertical on top of the silicon substrate. The inset represents a tilted image with 30 degrees and can see an accumulation of ZnO nanorods. This morphology of the ZnO Nanorods was confirmed by the reported data [19, 34]. The average diameter of single nanorods was measured within 100nm. This value is compared with AFM measurements of the grain size of the seed layer which is about 95 nm. These measurements confirm the formation phenomenon of the nanorod diameter which is influenced by the ZnO nanoparticle. This finding was reported elsewhere [34].

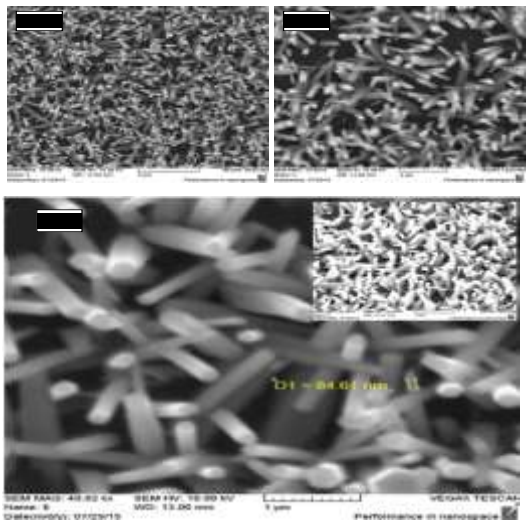

Figure 4: SEM images of ZnO NRs/SiO2/Si (111), hydrothermally synthesized at 85 °C for 2h, and with 30 mM seed layer concentration (Inset image is tilted 30°)

V. Energy dispersive spectroscopy (EDS)

The EDS analysis was performed to investigate the quality of the synthesized and annealed ZnO NRs film at 500 °C in the air. The spectrum is shown in Figure 5. There is a higher intensity energy peak corresponds to the silicon which is related to the silicon substrate. The observed Si peak was confirmed by other reported result [35]. The other peaks are corresponding to the oxygen (O) and zinc (Zn) elements. The chemical composition of the analyzed EDS spectrum is purely Zn and O with no other impurity was found. The average atomic percentage of the ZnO product is slightly rich in oxygen. Thus, the EDS analysis reveals that a high purity of ZnO NRs was grown. This purity of ZnO NRs was confirmed by my previous work [10, 17]. The present results were also found to be in good agreement with our XRD results.

VI. Optical properties of ZnO nanostructures

Figure 6 shows the optical absorbance spectrum of the annealed ZnO NRs film. The optical band gap was calculated using Tacu's plot [36] from the absorbance spectrum. The band gap was related to the absorption coefficient and incident photon (hν) and is given as (αhν).

$(\alpha h\nu)=B(h\nu-Eg)1/2$ (5)

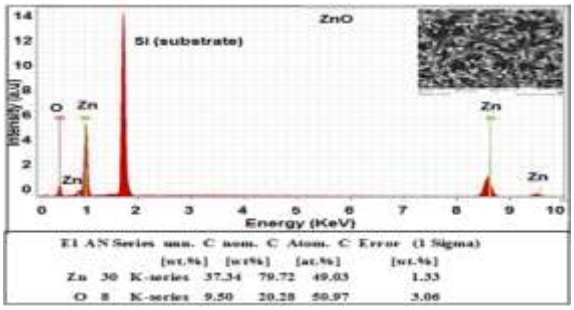

Figure 5: EDS spectrum of annealed ZnO NRs film with the Zn and O elements composition

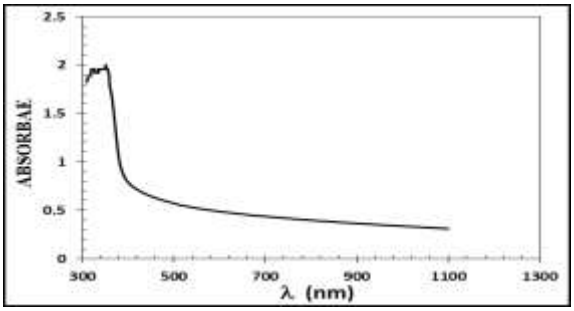

Figure 6: Absorbance spectrum of the annealed ZnO NRs film

Figure 7 shows plots of $(\alpha h\nu)2$ versus $(h\nu)$. The value of the optical band gap (Eg) was determined from the extrapolation of the best tangential to the curve. The optical band gap was found to be 3.2eV for the ZnO NRs annealed film which is quite close to the bulk ZnO band gap and is in good agreement with other reported data [37]. The slight decrease in band gap could be due to the annealing process of the film.

VII. Gas sensor fabrication

1) I-V Characteristics

Figure 8 shows the schematic illustration for ZnO NRs gas sensor device. The silicon substrate (111) was oxidized to SiO_2 (to use as an insulator) under oxygen flow through the tube furnace at a temperature of 1000 °C for one hour. The obtained thickness of the SiO_2 film was about 300 nm. The oxidation process is described in thesis work [38]. Silver paste contact was painted on top of the nanorods film like a pad. These are connected to copper wires to measure the current, voltage and resistance of the device using power supply and a picometer Keithley (model 616) as demonstrated in Fig 8.

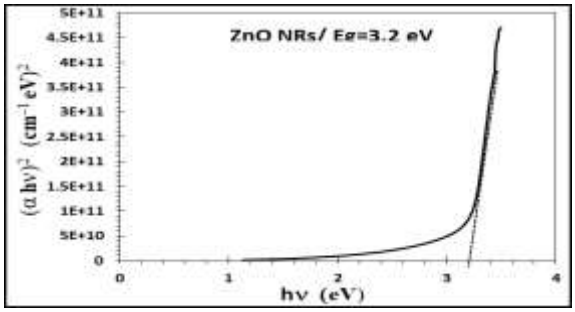

Figure 7: Tauc's plot of optical band gap calculation for the annealed ZnO NRs film

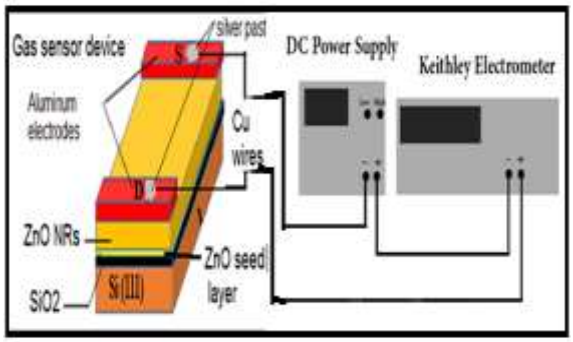

Figure 8: Schematic of a gas sensor device based on ZnO NRs film

The I-V characteristics were measured and shown in Figure 9. It shows a nonlinear relationship and rectifying behavior is observed. This behavior indicates that the Schottky barrier has formed at the metal-semiconductor contact. It is reported that the work function of ZnO (ϕ=5.2 eV) is larger than that of silver (ϕ=4.26 eV) [39]. Thus, the observed Schottky contact can be attributed to

the differences between ZnO and Ag work functions [40].

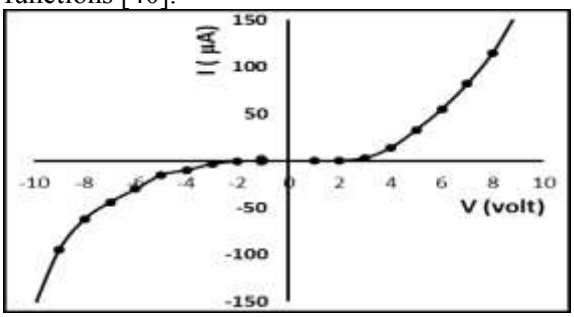

Figure 9: I-V characteristics for ZnO NRs /SiO2/Si (111), hydrothermally synthesized at seed layer concentration of 30 mM.

2) Methanol gas sensor properties

The gas sensing measurement was carried out using our homemade gas sensor system shown in Fig 10.

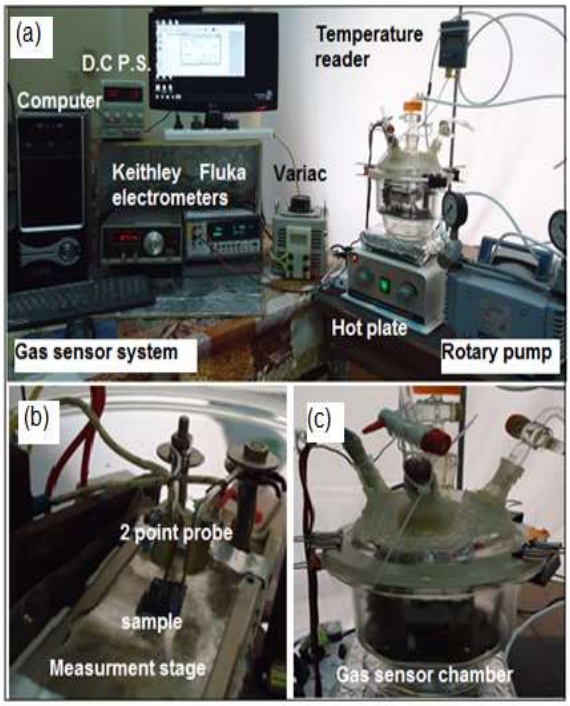

Figure 10: Photograph of the homemade gas sensor system; (a) complete setup; (b) measurement stage; and (c) glass reaction chamber/ (UOT).

Figure 11 shows a typical sensor response of ZnO NRs film towards methanol gas concentrations of 150, 200, 250 ppm and at a substrate temperature of 200 °C in a static process of sensing. A certain amount of ethanol liquid was injected through a rubber stopper by a syringe onto a pre-heating bottom of the known chamber volume. This can be done by placing a small heater with a low supply power under the chamber to maintain the methanol evaporation and reach the equilibrium condition and full the whole chamber. The concentration of the injected volume of methanol was calculated in ppm. The resistance of the film in the air was recorded firstly when the film is exposed to the air. This would be Ra (denoted as resistance at air). After resistance stability, the methanol liquid is injected and any change is registered in resistance due to the exposed gas. This resistance would be denoted as Rg (Due methanol gas). The sensitivity can be calculated by using the formula [41]:

$$S = Ra/Rg \quad (6)$$

Where Ra is greater than Rg for n-type ZnO film that interacting with reductive gas. This property makes the initial resistance to decrease when the ZnO film exposed to the ethanol gas as shown in Figure 11. So, the calculated sensitivity (S = Ra/Rg) versus time was drawn in Figure12 at various ethanol concentrations. From this figure, the sensitivity factor was calculated for the three response peaks using: S (Sensitivity) /1ppm (part per million) =1.5/150ppm= 0.01, 2/200pm=0.01, and 5/250ppm=0.02 .

It was found that the sensitivity of ZnO NRs film was gradually increased when the methanol concentration increased from 150-250 ppm as shown in Figure 13 .

The response and recovery time curves are shown in Figure 14 for the ZnO NRs film sensor towards methanol vapor at various concentrations. The value of the response and recovery time are estimated within the ranges of 40-60s and 60-80s respectively at methanol concentration of 150-250 ppm and at a substrate temperature of 200 °C .

From Figure 13, the sensitivity of the sensor at 250ppm is about 5. This value was found to be equivalent to the reported result [42]. It can also be seen from Figure 14 that the response and recovery time at methanol gas concentration of 200 ppm and temperature of 200 °C, are the 60s and 80 s, respectively. These values were found to be quite consistent with the reported data at 200 ppm and even at a higher temperature (300 °C) [43].

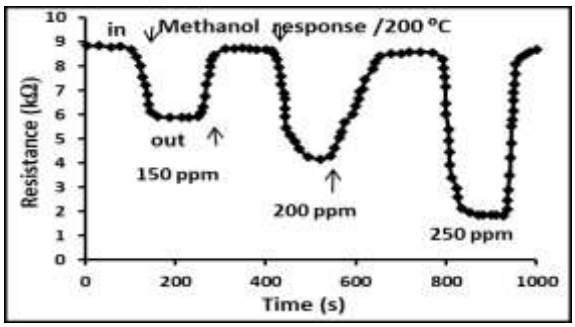

Figure 11: Sensor resistance versus time at various methanol concentrations.

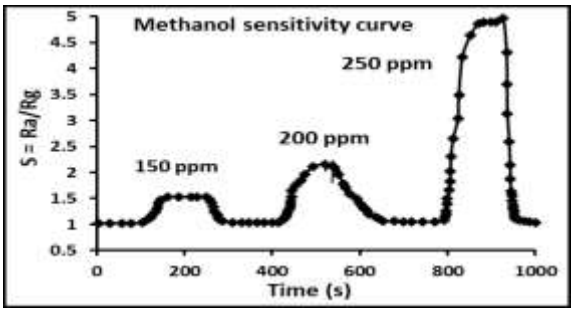

Figure 12: Sensor sensitivity versus time at various methanol concentrations.

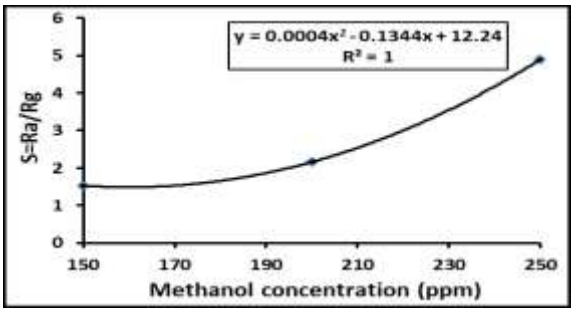

Figure 13: Sensor sensitivity versus methanol concentration.

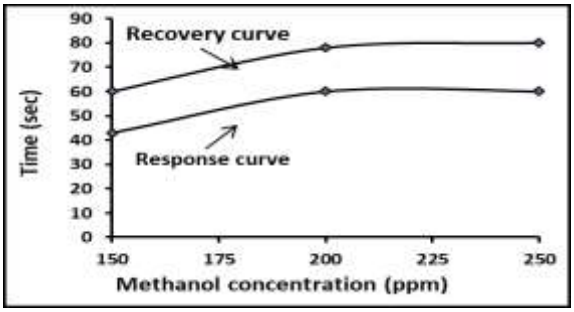

Figure 14: Response and recovery time curves versus various methanol concentrations.

4. Conclusion

ZnO nanostructures can be synthesized using a variety of techniques. Hydrothermal synthesis is amongst these techniques to easily produce ZnO nanostructures at low temperature and with a large scale. In the present study, structural, morphological, optical studies were carried out on the synthesized and annealed ZnO NRs. The XRD exhibited a pure polycrystalline ZnO NRs which was confirmed by the EDS analysis. The calculated energy gap was 3.2 eV also confirmed the ZnO structure. The ZnO NRs film reviled a good sensitivity to the methanol vapors with fast response and recovery time. It was also found that the sensitivity was about 5 for methanol vapor concentration of 250 ppm at an operating temperature of 200 °C. ZnO NRs seems to be a promising semiconducting material for methanol vapor detection. The application of methanol gas sensor can be used for gas leakage in the industry and chemical laboratories.

Acknowledgment

I'm sincerely grateful to the University of Technology and the head of the Applied Science research unit (ASRU) and all the staff for this great opportunity that they gave me in order to finish this work.

References

[1] P. Nunes, B. Fernandes, E. Fortunato, P. Vilarinho, and R. Martins, "Performances presented by zinc oxide thin films deposited by spray pyrolysis", Journal of Thin Solid Films, Vol. 337, pp. 176–179, January, 1999.

[2] T. P. Chou, Q. F. Zhang, G. E. Fryxell and G. Z. Cao, "Hierarchically structured ZnO film for dye-sensitized solar cells with enhanced energy conversion efficiency," Advanced Materials, Vol. 19, No. 18, pp. 2588-2592, September, 2007.

[3] U. Rau, and M. Schmidt, "Electronic properties of ZnO/CdS/Cu(In,Ga)Se2 solar cells aspects of heterojunction formation", Journal of Thin Solid Films Vol. 387, pp.141–146, May, 2001.

[4] T. Soki, Y. Hatanaka, and D. Look, "ZnO diode fabricated by excimer-laser doping", Appl. Phys. Lett. Vol. 76, No. 22, pp. 3257-3258, May, 2000.

[5] U. Alver, T. Kılınç, E. Bacaksız, T. Kucukomerogla, S. Nezir, I.H. Mutlu, and F. Aslan, "Synthesis and characterization of spray pyrolysis zinc oxide microrods", Thin Solid Films Vol. 515, pp. 3448–3451, February, 2007.

[6] M.H. Huang, Y. Wu, H. Feick, N. Tran, E. Weber, and P. Yang, "Catalytic growth of zinc oxide nanowires by vapour transport", Adv. Mater. Vol. 13, pp. 113-116, January, 2001.

[7] G.K. Paul, and S.K. Sen, "Sol-gel preparation, characterization, and studies on electrical and thermoelectrical properties of gallium doped zinc oxide films", Mater. Lett. Vol. 57, pp. 742–746, December 2002.

[8] E.M. Kaidashev, M. Lorenz, H. V. Wenckstern, A. Rahm, H.-C. Semmelhack, K.-H. Han, G. Benndorf, C. Bundesmann, H. Hochmuth, and M. Grundmann, "High electron mobility of epitaxial ZnO thin films on c-plane sapphire grown by multistep pulsed-laser deposition", Appl. Phys. Lett. Vol. 82, pp. 3901-3903, June 2003.

[9] M.J.H. Henseler, W.C.T. Lee, P. Miller, S.M. Durbin, and R.J. Reeves, "Optical and photoelectrical properties of ZnO thin films and the effects of annealing", J. Cryst. Growth Vol. 287, pp. 48-53, January, 2006.

[10] A. D. Faisal, "Synthesis of ZnO comb-like nanostructures for high sensitivity H2S gas sensor

fabrication at room temperature", Bull. Mater. Sci., Vol. 40, No. 6, pp. 1061–1068, October, 2017.

[11] J.M. Bian, X.M. Li, X.D. Gao, W.D. Yu, and L.D. Chen, "P-type ZnO films by monodoping of nitrogen and ZnO-based p-n homojunction", Appl. Phys. Lett. Vol. 85, pp. 4070 – 4072, December, 2004.

[12] H. Zeng, J. Cui, B. Cao, U. Gibson, Y. Bando, and D. Golberg, "Electrochemical deposition of ZnO nanowire arrays: organization, doping, and properties", Sci. of Adv. Mater. Sci. Vol. 2, 336–358, September, 2010.

[13] D. P. Singh, "Synthesis and growth of ZnO nanowires", Sci. Adv. Mater. Vol. 2, pp. 245–272, October, 2010.

[14] H. Zhang, N. Du, B. Chen, D. Li, and D. Yang, "Carbon nanotube-ZnO nanosphere heterostructures: low-temperature chemical reaction synthesis, photoluminescence, and their application for room temperature NH3 gas sensor", Sci. Adv. Mater. Vol. 1, pp. 13–17, April, 2009.

[15] X. Ren, and C. Jiang, "Synthesis of ZnO nanotube arrays and heterostructures of Cu–ZnO coaxial nanotubes by electrodeposition–oxidation method", J. Nanosci. Nanotechnol. Vol. 10, pp. 5093–5098, August 2010.

[16] K. Zhu, Z. Yan, and W. Chen, "Fabrication of hourglass-like ZnO particles with enhanced blue emission", J. Nanosci. Nanotechnol. Vol. 10, pp. 6594–6598, October, 2010.

[17] A. D. Faisal, "Optimization of CVD parameters for long ZnO NWs grown on ITO/glass substrate", Bull. Mater. Sci., Vol. 39, No. 7, pp. 1635–1643, 2016.

[18] P. X. Gao, C.S. Lao, W.L. Hughes, and Z.L. Wang, "Three-dimensional interconnected nanowire networks of ZnO", Chem. Phys. Lett. Vol. 408, pp. 174–178, June, 2005.

[19] A. D. Faisal, "Influence of seed layer on morphology and structure of ZnO nanowires synthesized on silicon via hydrothermal method", Al-Mustansiriyah Journal of Science, Vol. 27, No 3, pp. 62-67, 2016.

[20] K. Ramamoorthy, C. Sanjeeviraja, K. Sankaranarayanan, P. Misra, and L.M. Kukreja, "Development of a novel high optical quality ZnO thin films by PLD for III–V opto-electronic devices", Curr. Appl. Phys. Vol. 6, pp. 103-108, December, 2006.

[21] J.M. Khoshman, and M.E. Kordesch, "Optical constants and band edge of amorphous zinc oxide thin films", Thin Solid Films Vol. 515 Issue 18, pp. 7393–7399, June, 2007.

[22] K. Zheng, Q.M. Xue, D. Guo, S. Liu, and E.G. Wang, "Ultra-thin zinc oxide film on Mo(100)", Thin Solid Films Vol. 515, Issue 18, pp. 7167-7170, June, 2007.

[23] F. Kadi Allah, S. YapiAbé, C.M. Nunez, A. Khelil, L. Cattin, M. Morsli, J.C. Bernède, A. Bougrine, M.A. del Valle, and F.R. Diaz, "Characterisation of porous doped ZnO thin films deposited by spray pyrolysis technique", Appl. Surf. Sci. Vol. 253, pp. 9241–9247, September, 2007.

[24] C.S. Barret, and T.B. Massalski, "Structure of Metals", Pergamon Press, Oxford, New York, 1980.

[25] B.D. Cullity, and S.R. Stock, "Elements of X-Ray Diffraction", Third Ed., Prentice-Hall, New York, 2001.

[26] Q. Zhou, J. Z. Wen, P. Zhao, and W. A. Anderson," Synthesis of vertically-aligned zinc oxide nanowires and their application as a photocatalyst," Nanomaterials, Vol. 7, Issue 9, pp. 1-13, January, 2017.

[27] J. Fan, T. Li, and H. Heng, "Hydrothermal growth of ZnO nanoflowers and their photocatalyst application," Bull. Mater. Sci., Vol. 39, No. 1, pp.19–26, 2016.

[28] R. S. Sabry, B. M. Ahmed, and T. A. A. Hassan," Simple hydrothermal synthesis of the ZnO hexagonal nanotubes", Australian Journal of Basic and Applied Sciences, Vol.10 (18), pp.303-309, 2016.

[29] B. K. Rohidas B., Y.-J. Hsu, Y.-F. Lin, and S.-Y. Lu," Hydrothermal synthesis, characterizations and photoluminescence study of single crystalline hexagonal ZnO nanorods with three-dimensional flowerlike microstructures", Superlattices and Microstructures Vol. 69, pp.239–252, 2014.

[30] R. B. Kale, Y.J. Hsu, Y. F. Lin and S.Y. Lu, "Hydrothermal synthesis, characterization and photoluminescence study of single crystalline hexagonal ZnO nanorods with three dimensional flowerlike microstructures", Superlattices and Microstructures, Vol. 69, pp. 239-252, 2014.

[31] E. Darezereshki, M. Ranjbar, and F. Bakhtiari, "One-step synthesis of maghemite (γ-Fe2O3) nanoparticles by a wet chemical method," Journal of Alloys and Compounds, Vol. 502, pp.257-260, 2010.

[32] C. Suryanarayana , and G. Norton. X-Ray Diffraction: A Practical Approach. Springer Science + Business Media, LLC, 233 Spring Street, New York, NY 10013, USA: Plenum Press; 1998.

[33]Y. T. Prabhu, K. V. Rao, V. Sesha S. Kumar, and B. S. Kumari, " X-Ray Analysis by Williamson-Hall and size-train plot methods of ZnO nanoparticles with fuel variation ", World Journal of Nano Science and Engineering, Vol. 4, pp.21-28, 2014.

[34] Z. H. Ibupoto, K. Khun, M. Eriksson, M. Alsahi, M. Atif, A. Ansari and M. Willander, "Hydrothermal growth of vertically aligned ZnO nanorods using a biocomposite seed layer of ZnO nanoparticles", Materials, Vol. 6, pp. 3584-3597, 2013.

[35] Y. I. Jung, B. Y. Noh, Y. S. Lee, S. H. Baek, J. H. Kim Visible emission from Ce-doped ZnO nanorods grown by hydrothermal method without a post thermal annealing process, Nanoscale Research Letters Vol. 7, Issue 43, pp. 1-5, 2012. DOI: 10.1186/1556-276X-7-43

[36] F. Urbach, "The long-wavelength edge of photographic sensitivity and of the electronic

absorption of solids", Phys. Rev., Vol. 92, pp. 1324, 1953.

[37] G. K. Mani, and J. B. B. Rayappan, "A highly selective room temperature ammonia sensor using spray deposited zinc oxide thin film", Sensor and Actuators B, Vol. 183, pp. 459-466, 2013.

[38] M. Majhi, " Growth and characterization of SiO2 thin film on silicon substrates", MSc. Thesis, National Institute of Technology, Rourkela, Rourkela-769008, Orissa, India, 2013.

[39] Z. Yin, X. Wang, F. Sun, X. Tong, C. Zhu, Q. Lv, D. Ye, S. Wang, W. Luo and Y. Huang, " Aligned hierarchical Ag/ZnO nano-hetrostructure arrays via electrohydrodynamic nanowire template for enhanced gas-sensing properties", Scientific Report, [7-12206], pp. 1-10, 2017. DOI:10.1038/s41598-017-12553-7.

[40] L. Liao, Z. Zhang, B. Yan, Z. Zheng, Q. L. Bao, T. Wu, C. M Li, Z. X. Shen, J. X. Zhang, H. Gong, J. C. Li and T. Yu, "Multifunctional CuO nanowire devices: P-type field effect transistors and CO gas sensor, Nanotechnology, Vol. 20, pp. 1-6, Dec. 2009.

[41] R. Kumar, O. Al-Dossary, G. Kumar, and A. Umar, "Zinc oxide nanostructures for NO_2 gas-sensor applications: A Review", nano-micro Lett. Vol.7 (2), pp.97-120, 2015.

[42] B.A.Vessalli, C.A.Zito, T.M.Perfecto, D.P.Volanti and T. Mazon, "ZnO nanorods/graphene oxide sheets prepared by chemical bath deposition for volatile organic compounds detection," J. of Alloys and Compounds Vol. 696, pp. 996-1003, 2017.

[43] N.Banerijee, K. Dutta, H.Misr and P. Bhattacharcharyya," Capacitive mode methanol sensing by ZnO nanorods based devices", Int. J. Material ,Mechanics and Manufacturing Vol.5, No. 2, 2017.